愛知工業大学研究報告
第２８号　平成５年

Formation Dynamics of Excited Components in ArF Excimer Laser Discharge

ArF エキシマレーザ放電における励起種の生成機構

古橋秀夫[†]　内田悦行[†]
Hideo FURUHASHI　Yoshiyuki UCHIDA

Abstract *Time-resolved density measurements of excited components in a discharge pumped ArF excimer laser were performed using laser absorption probing with a cw dye laser pumped by a Ar^+ laser. The dependence of the He^* $2p^3P$ densities on the gas parameters were measured. The relationships between laser output power and the number densities of He^* are discussed. The relationships between the laser output power and the formation rate of Ar^+ ions by Penning ionization with He^* atoms are also discussed.*

1. Introduction

Discharge pumped excimer lasers are high power and high efficiency coherent light sources in the ultraviolet (UV) region of spectrum. Possessing the shortest wavelength (193nm) among rare gas halide lasers , the ArF lasers have the highest photon energy, so that they are capable of initiating photochemical reactions by a single photon. They have numerical applications such as photochemistry, photolithography of very large scale devices, photochemical vapor deposition, and spectroscopy[1-6]. Many remarkable advances have been made in excimer lasers for high power or for high efficiency.

On the other hand, the investigations of excitation mechanism by computer modeling have been reported[7-10]. They have currently aroused great interest as a useful means for investigating the physical process occurring in the active medium, the influence of the large number of parameters on the lasing pulse and as a helpful tool for the optimization and development of various laser designs. But most of the computer modeling involve several assumptions and parameters obtained by the simulation are different from those of actual laser devices in some points. In order to confirm the analyses of the kinetic model of the lasing by computer modeling and understand physico-chemical process in discharge plasma, experimental determination of plasma discharge parameters in excimer laser discharge is necessary. Reliable diagnostic data for the discharge plasma is of great importance for the further development of excimer laser physics. Especially it is important to measure the particle number densities of excited atoms and ions and study their roles on laser performance and basic plasma-chemical reactions in laser active medium.

Thanks to its high spectral, temporal, and spatial resolution, dye laser absorption spectroscopy is a useful method for measuring particle number densities in excimer lasers, and makes it possible to study the dynamics of formation and decay of excited atoms, ions, and molecular complexes. As for XeCl excimer lasers, the quantitative studies of formation dynamics of excited components in the discharge

[†]情報通信工学科

plasma from the data of dye laser absorption probing have been carried out[11-14]. However, those on ArF excimer lasers have not been reported.

In this paper, the absorption coefficient of the He* 587.6nm line ($2p^3P \rightarrow 3d^3D$) in the ArF excimer laser discharge was measured using laser absorption spectroscopy with a cw ring dye laser as a light source. Time-resolved He* number densities at the $2p^3P$ level were obtained from the measured absorption coefficient for various gas mixtures. We discuss the role of buffer gas He on the laser performance from the viewpoint of the formation kinetics of excimer molecules.

2. Principle of measurement

The well known derivation method of the atom density at the lower level from the absorption coefficient of line is described by Mitchell and Zemansky[15]. The function of the incident light of frequency ν that passes through an absorbing layer of thickness L is given by

$$\frac{I_\nu}{I_{\nu_0}} = exp(-k\nu L) \qquad (1)$$

where Iν and Iν_0 are the transmitted light intensities with and without absorption at a frequency ν respectively, and kν is the absorption coefficient as a function of frequency. The integral of the absorption coefficient is expressed by[15]

$$\int k\nu d\nu = \frac{1}{8\pi}\lambda_0^2 \frac{g_2}{g_1} NA \qquad (2)$$

where λ_0 is the wavelength of the transition and g_1 and g_2 are the statistical weights of lower and upper levels respectively, N is the atom density at the lower level and A is the Einstein coefficient. It is assumed that the density at the upper level is much smaller than that at the lower level. Therefore, by using the measured absorption profile, the atom density N at the lower level is calculated.

3. Experimental Apparatus

The object of the investigations is the discharge pumped excimer laser constructed by ourselves. Figure 1 shows the cross-sectional view of the excimer laser. This laser is of capacitor-transfer with automatic UV preionization type, controlled by an EG&G LS 4111 thyratron switch. The storage capacitor C_1 and the peaking capacitor C_2 contain 40 and 24 doorknob ceramic capacitors of 1.7nF, and their capacitances are 68nF and 40.8nF respectively. The driving voltage is 30kV. The stainless electrodes are designed for Ernst profile[16]. The length of the discharge gap is 60cm and the transverse cross section of the discharge is 0.8cm (width) ×1.8cm (height). For preionization sparks, an array of small 72 nickel pin gaps (2mm) is located 1.2cm apart from the cathode in two lines. The optical cavity consists of a highly reflective dielectric-coated external mirror and uncoated quartz window of the laser tube, separated by 90cm.

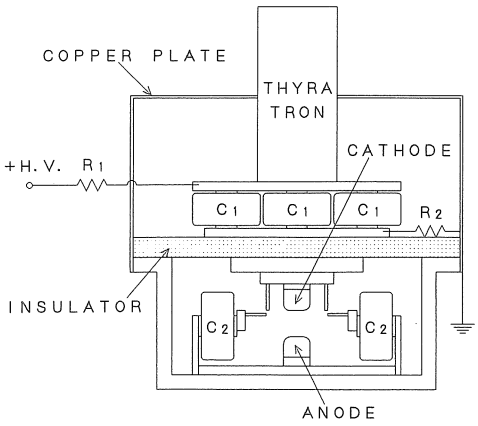

Fig. 1 Cross-sectional view of the laser.

Figure 2 shows the schematic diagram of the experimental apparatus. The laser beam of the ring dye laser was used as the light source for absorption spectroscopy. The ring dye laser (Coherent Model CR-699-21) produced tunable single-frequency radiation. The cw argon ion laser (Coherent Innova 90-5) was used to optically pump the dye (Rhodamine 6G). The tunable wavelength of the dye laser was in the range between 570nm and 610nm at a linewidth of 2GHz (with a three-plate birefringent filter). The diameter of the laser beam waist was about

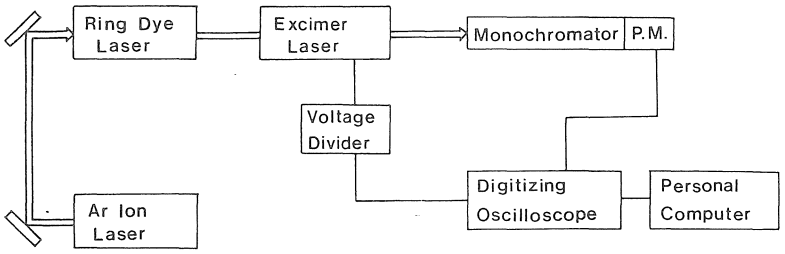

Fig. 2 Schematic diagram of experimental apparatus.

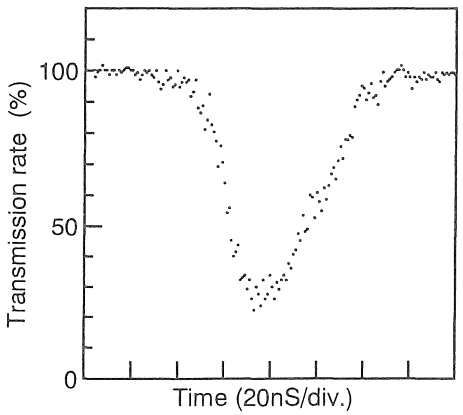

Fig. 3 Transient transmission waveform near the 587.6nm line center in the ArF excimer laser discharge using gas mixture of F_2:Ar:He = 0.2:10:89.8 at the total pressure of 2.5atm.

3mm and its power was about 600mW.

The output of the ring dye laser was tuned to the He* 578.6nm ($2p^3P \rightarrow 3d^3D$) line. The laser beam passed through the plasma and was detected with a monochromator and a photomultiplier. The data of 64 measurements at one wavelength were averaged by using a digitizing-oscilloscope before subsequent transferral to a microcomputer, and permanent storage on floppy disks. The measurements of the voltage pulses were made with a handmade $CuSO_4$ voltage divider. The voltage between the two electrodes was used as triggering signals of the digitizing-oscilloscope.

From the transient transmission waveform at a frequency ν, the transmitted light intensities I_ν with absorption and I_{ν_0} without absorption at a frequency ν were measured. From the ratio I_ν / I_{ν_0}, the absorption coefficient $k\nu$ at a frequency ν was obtained using equation (1). From the obtained absorption coefficient profile, the time-resolved He*($2p^3P$) density was calculated using equation (2).

4. Results and discussion

The concentration of excimer molecules is the main parameter of the active medium of an excimer laser. The main ArF* excimer formation channels in F_2/Ar/He mixture considered and reported with computer modeling are three body ion-ion recombination and harpooning reaction shown below[17–19]

$$Ar^+ + F^- + He \rightarrow ArF^* + He \qquad (3)$$

$$Ar^* + F \rightarrow ArF^* \qquad (4)$$

and it is considered that Penning ionization shown below is a reaction of the Ar^+ formation [19,20].

$$Ar + He^* \rightarrow Ar^+ + He + e \qquad (5)$$

Hence, Ar^+, F^-, Ar*, and He* play important roles in ArF* excimer formation.

Figure 3 shows an example of the transient transmission waveform near the line center (587.6nm) in the ArF excimer laser using gas mixture of F_2/Ar/He. The gas mixture was F_2:Ar:He = 0.2:10:89.8 and the total pressure was 2.5atm. In the case of measurements of He* ($2p^3P$), since the energy levels of He* atoms in the $2p^3P_0$, $^3P_1$ and $^3P_2$ states were close and the line absorption line profiles connecting with the upper level overlapped one another[12,13],

the densities could not be obtained individually. Therefore, the total densities of He* atoms in the $2p^3P_0$, $^3P_1$ and $^3P_2$ states were calculated by integrating the total line profile directly and using equation (2).

Figure 4 shows an example of the measured time dependence of He* densities. The time origin corresponds to the start of the main discharge. The gas mixture was F_2:Ar:He = 0.2:10:89.8 and the total pressure was 2.5 atm.

Figure 5 shows the temporal behavior of the He* density, the emission of the ArF* excimer and the voltage across the discharge electrodes. The first sharp peak of the voltage trace is due to the short of the preionization gaps. After break down, the discharge current rises up and following that the He* density increases. About 40ns and 20ns time lags of the peak of the emission of the ArF* excimer are observed behind the break down and the peak of the He* density respectively. This is due to the time lag of ArF* excimer formation.

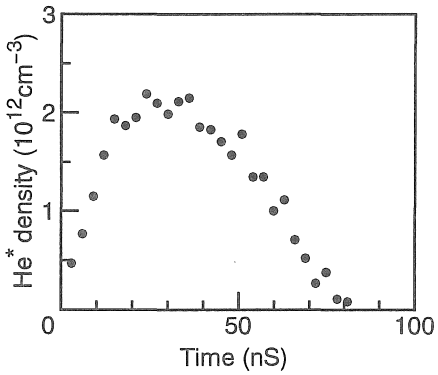

Fig. 4 Time-resolved He* ($2p^3P$) density in the ArF excimer laser discharge using gas mixture of F_2:Ar:He = 0.2:10:89.8 at the total pressure of 2.5atm.

Figure 6 shows the He* density as a function of F_2 fractional concentration. The He* densities were measured for three kinds of F_2 fractional concentration of 0.1%, 0.2% (optimum),and 0.3%. The Ar fractional concentration and the total pressure were kept 10% and 2.5atm respectively. Though the He* density increases very slowly with the increase in F_2, there is little influence of F_2 fractional concentration on the He* density within the F_2 fractional concentration of 0.3%. On the other hand, F_2 fractional concentration influences on the laser output power.

In this case the Ar fractional concentration is fixed and the electron density affects on the He* density. In the early glow discharge, the electron density grows rapidly because the rate of electron production through the reaction

$$Ar + e \rightarrow Ar^+ + 2e \qquad (6)$$

is a very strong function of the effective field in the discharge as compared with the rate of dissociative attachment of F_2. But in the middle of the glow discharge the dissociative attachment of F_2 does indeed become an important process because of drastic cooling of electron temperature[21]. Since the He* density increases

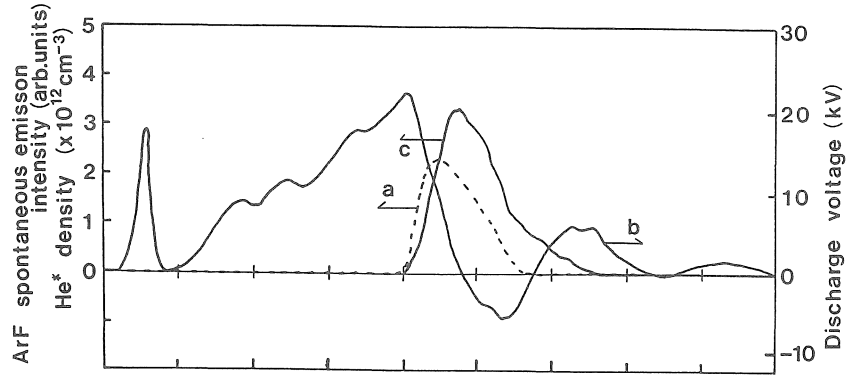

Fig. 5 Temporal behavior of the He*density (a), the discharge voltage (b), and the emission of ArF* excimer (c) in the ArF excimer laser discharge using gas mixture of F_2:Ar:He = 0.2:10:89.8 at the total pressure of 2.5atm. Horizontal axis : 50ns/div.

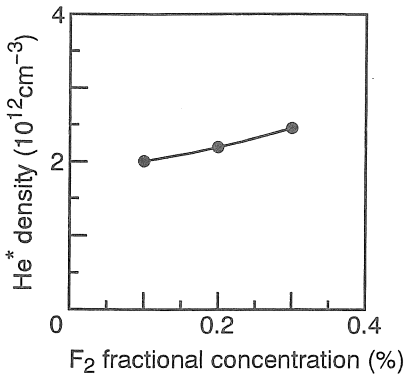

Fig. 6 He* density as a function of F_2 fractional concentration. Ar fractional concentration and the total pressure are 10% and 2.5atm respectively.

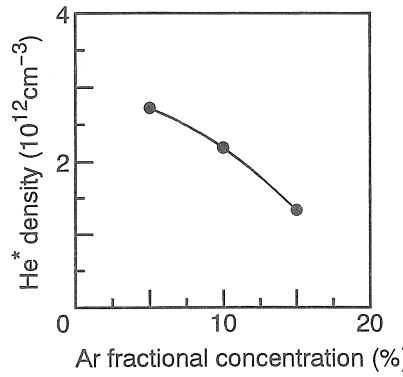

Fig. 7 He* density as a function of Ar fractional concentration. F_2 fractional concentration and the total pressure are 0.2% and 2.5atm respectively.

rapidly after break down and has the peak in the early discharge as shown in Figure 5, the influence of F_2 fractional concentration on the peak of He* density is rather small, as described above.

When F_2 fractional concentration is increased, the reactions described below affect on the laser performance. Formations of ArF* excimer by three body ion-ion recombination (3) and harpooning reaction (4) become active. On the other hand, quenching of ArF* excimer shown below[17,18]

$$ArF^* + F_2 \rightarrow \text{Products} \qquad (7)$$

and photoabsorption of 193nm (ArF*) shown below[22,23]

$$F_2 + h\nu \rightarrow F + F \qquad (8)$$
$$F^- + h\nu \rightarrow F + e \qquad (9)$$

also become active, and addition of F_2 affects on the laser performance.

Figure 7 shows the He* density as a function of Ar fractional concentration.The F_2 fractional concentration and the total pressure were kept 0.2% and 2.5atm respectively. The He* densities were measured for three kinds of Ar fractional concentration, 5%, 10% (optimum), and 15%. The He* density decreases rapidly with the increase in the Ar fractional concentration.

When Ar concentration is increased, Penning ionization (5) becomes active and the decay rate of the He* by Ar^+ ions formation increases. The dominant electron formation processes are the direct and two step ionization of Ar i.e.

$$Ar + e \rightarrow Ar^+ + 2e \qquad (10)$$
$$Ar + e \rightarrow Ar^* + e \qquad (11)$$
$$Ar^* + e \rightarrow Ar^+ + 2e \qquad (12)$$

and the energies required for those reactions are 15.8eV, 11.5eV, and 4.3eV respectively. Hence, the discharge impedance decreases at higher Ar partial pressure, and at the same time the electron energy decreases owing to the collision of the electrons with Ar atoms. Lower energy electrons increase and the formation of He* atoms decreases.

As shown in the three body ion-ion recombination (3), Ar^+ ions are concerned with the formation of ArF* excimer. Figure 8 shows the formation rate of Ar^+ ions in the reaction (5) as a function of Ar fractional concentration. The formation rate of Ar^+ ions was calculated on the assumption that the overall density of He* atoms is proportional to the density of He* at the level of $2p^3P$. The dependence of the peak laser output power is also presented. The F_2 fractional concentration and the total pressure were kept 0.2% and 2.5 atm respectively.

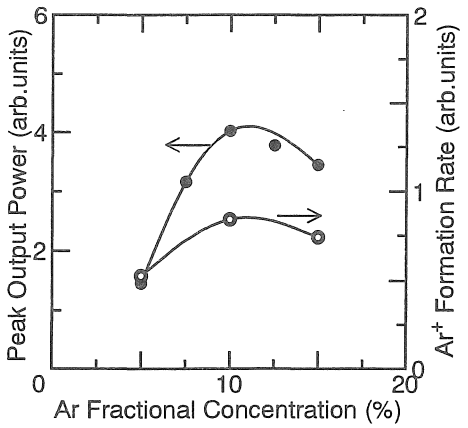

Fig. 8 Dependence of peak output power (•) and Ar^+ formation rate (○) for Ar fractional concentration.

With the increase in the Ar fractional concentration, the peak laser output power increases until reaching 10% and then decreases. The formation rate of Ar^+ ions in the reaction (5) has a similar disposition to that of the peak laser output power. It seems that He^* atoms have some relations with the ArF excimer laser performance through Ar^+ formation reaction (5).

5. Conclusion

By using absorption spectroscopy with a ring dye laser pumped by an argon ion laser as a light source, the measurements of the time-resolved particle number of the He^* ($2p^3P$) density in the ArF excimer laser discharge have been carried out. The dependence of the He^* densities as a function of Ar fractional concentration and F_2 fractional concentration has been investigated. It was found that the peak of the He^* density was influenced conspicuously by Ar fractional concentration in comparison with F_2 fractional concentration. He^* atoms may play important roles in the formation channel of Ar^+ ions and may be concerned with the laser peak output power. For further quantitative study of ArF excimer formation, the measurements of other excited components (Ar^*, Ar^+, F^-) densities and the electron density remain as future tasks of importance.

REFERENCES

1) H. Hemmati and G. J. Collins, IEEE J. Quantum Electron., vol. QE-16, pp. 1014–1016, Oct. 1980.

2) A. W. McCown and J. G. Eden, Appl. Phys. Lett., vol. 40, pp. 371–373, Sep. 1981.

3) T. F. Deutsch, J. C. C. Fan, G. W. Turner, R. l. Chapman, D. J. Ehrilich, and R. M. Osgood, Jr., Appl. Phys. Lett., vol. 38, pp. 144–146, Feb. 1981.

4) T. F. Deutsch, D. J. Ehrlich, D. D. Rathman, D. J. Silversmith, and R. M. Osgood, Jr., Appl. Phys. Lett., vol. 39, pp. 825–827, Nov. 1981.

5) R. W. Andreatta, C. C. Abele, J. F. Osmundsen, and J. G. Eden, Appl. Phys. Lett., vol.40, pp. 183–185, Jan. 1982.

6) D. H. Lowndes, D. B. Geohegan, D. Eres, S. J. Pennycook, D. N. Mashburn, and G. E. Jellison, Jr., Appl. Phys. Lett., vol. 52, pp. 1868–1870, May 1988.

7) M. Maeda, A. Takahashi, T. Mizunami, and Y. Miyazoe, Jpn. J. Appl. Phys. Part 1, vol. 21, pp. 1161–1169, May 1982.

8) M. Ohwa and M. Obara, J. Appl. Phys., vol. 59, pp. 32–41, Jan. 1986.

9) V. M. Baginskii, P. M. Golovinskii, V. A. Ounilychev, A. I. Milanich, A. S. Soroka, and A . I. Shchedrin, Sov. J. Quantum Electron, vol. 16, pp. 488–493, Apr. 1986.

10) G. Stielow, Th. Hammer, and W. Botticher, Appl. Phys. B, vol. 47, pp. 333–342, Jun. 1988.

11) V. E. Peet and A. B. Treshchalov, Sov. J. Quantum Electron, vol. 15, pp. 1613–1619, Dec. 1985.

12) A. B. Treshchalov, V. E. Peet, and V. T. Mihkelsoo, IEEE J. Quantum Electron, vol. QE-22, pp. 51–57, Jan. 1986.

13) P. Kh. Miida, V. E. Peet, R. A. Sorkina, E. E. Tamme, A. B. Treschalov, and A. V. Shermun, Sov. J. Quantum Electron, vol. 16, pp. 488–493, Nov. 1986.

14) A. B. Treshchalov and V. E. Peet, IEEE J. Quantum Electron, vol. QE-24, pp. 169–176, Feb. 1988.

15) A. C. G. Mitchell and M. W. Zemansky, Resonance Radiation and Excited Atoms, Cambridge University Press, 1934.

16) G. J. Ernst, Opt. Commun., vol. 47, pp. 47–51, Aug. 1983.

17) N. G. Basov, V. A. Donilychev, V. A. Dolgikh, O. M. Kerimov, V. S. Lebedev, and A. G. Molchanov, Sov. J. Quantum Electron, vol. 9, pp. 593–597, May 1979.

18) M. R. Flannery and T. P. Yang, J. Chem. Phys., vol. 73, pp. 3239–3245, Oct. 1980.

19) M. Ohwa and M. Obara, J. Appl. Phys., vol. 63, pp. 1306–1312, Mar.1988.

20) Y. W. Lee, E. Matsui, F. Kannari, and M. Obara, IEEE Transactions on Electron Devices, vol. 36, pp. 2053–2066, Sep.1989.

21) T. Mochizuki, K. Hirata, H. Ninoyama, K. Nakamura, K. Maeda, S. Horiguchi, and Y. Fujiwara, Opt. Commun., vol. 72, pp. 302–304, Aug. 1989.
22) R. J. Robinson and S. Geltman, Phys. Rev., vol. 153, pp. 4–8, Jan. 1967.
23) D. W. Trainor and J. H. Jacob, Appl. Phys. Lett., vol. 37, pp. 675-677, Oct. 1980.

(受理　平成5年3月20日)